Evidence of Dynamic Crustal Deformation in Tohoku, Japan, From Time-Varying Receiver Functions

Porritt, R. W.

Yoshioka, Shoichi

(Citation)
Tectonics,36(10):1934-1946

(Issue Date)
2017-10

(Resource Type)
journal article

(Version)
Version of Record

AGU PUBLICATIONS

Tectonics

RESEARCH ARTICLE
10.1002/2016TC004413

Special Section:
An Appraisal of Global Continental Crust: Structure and Evolution

Evidence of Dynamic Crustal Deformation in Tohoku, Japan, From Time-Varying Receiver Functions

R. W. Porritt[1,2,3] and S. Yoshioka[1,4]

[1]Research Center for Urban Safety and Security, Kobe University, Kobe, Japan, [2]Department of Geosciences, University of Arizona, Tucson, AZ, USA, [3]Institute for Geophysics, University of Texas at Austin, Austin, TX, USA, [4]Department of Planetology, Graduate School of Science, Kobe University, Kobe, Japan

Abstract Temporal variation of crustal structure is key to our understanding of Earth processes on human timescales. Often, we expect that the most significant structural variations are caused by strong ground shaking associated with large earthquakes, and recent studies seem to confirm this. Here we test the possibility of using *P* receiver functions (PRF) to isolate structural variations over time. Synthetic receiver function tests indicate that structural variation could produce PRF changes on the same order of magnitude as random noise or contamination by local earthquakes. Nonetheless, we find significant variability in observed receiver functions over time at several stations located in northeastern Honshu. Immediately following the Tohoku-oki earthquake, we observe high PRF variation clustering spatially, especially in two regions near the beginning and end of the rupture plane. Due to the depth sensitivity of PRF and the timescales over which this variability is observed, we infer this effect is primarily due to fluid migration in volcanic regions and shear stress/strength reorganization. While the noise levels in PRF are high for this type of analysis, by sampling small data sets, the computational cost is lower than other methods, such as ambient noise, thereby making PRF a useful tool for estimating temporal variations in crustal structure.

Key Points:
- The strong shaking of the Tohoku-oki earthquake-induced fluid migration and stress reorganization in the Tohoku inland region
- Synthetic PRF tests indicate structural change can be mapped by variations in PRF
- Stations showing high anticorrelation after the Tohoku-oki earthquake are well distributed throughout Tohoku

Supporting Information:
- Supporting Information S1

Correspondence to:
R. W. Porritt,
rporritt@ig.utexas.edu

Citation:
Porritt, R. W., & Yoshioka, S. (2017). Evidence of dynamic crustal deformation in Tohoku, Japan, from time-varying receiver functions. *Tectonics*, *36*, 1934–1946. https://doi.org/10.1002/2016TC004413

Received 7 NOV 2016
Accepted 4 SEP 2017
Accepted article online 12 SEP 2017
Published online 5 OCT 2017

1. Introduction

The 11 March 2011 *M*9 Tohoku-oki earthquake is among the largest and best recorded megathrust earthquakes to date. This earthquake provides a unique data set to investigate, among other questions, the effect of strong ground shaking in a well-instrumented arc environment. The Japanese Islands, most notably northeastern Honshu, directly west of the main shock (Figure 1), are densely instrumented by displacement sensitive GPS receivers (GEONET), velocity-proportional seismometers (Hi-net and F-net), and strong motion accelerometers (K-net and KiK-net); some of these instruments are deployed in boreholes, yielding recordings with very low noise levels. The recordings nearest the fault plane show peak ground motions of up to ~3 g in acceleration, ~25 cm/s velocity (e.g., Brenguier et al., 2014), and ~5 m displacement (e.g., Pollitz et al., 2011).

Geodetically inferred slip models suggest the main slip ranged from 33 m to 60 m (e.g., Hayes, 2011; Pollitz et al., 2011; Simons et al., 2011) and largely ruptured updip from a maximum depth of ~30 km to the seafloor trench with peak slip at ~10 km depth. However, these geodetically inferred models from displacement records typically reflect the relatively long period crustal deformation. Velocity seismic records at short periods to high frequencies (0.05–2 Hz) tend to show downdip rupture by the backprojection method, initially toward the northwest and then to the south (Kiser & Ishii, 2012; Meng et al., 2011). This discrepancy, discussed in Koper et al. (2011) and Lay et al. (2011), indicates differences in our observations of Earth processes based on measuring tool, frequency-dependent effects, where measurements are made, and biases built into different methodologies.

Nonetheless, all analyses agree that northeastern and central Honshu, and more specifically, the Tohoku, Kanto, and Chubu regions, experienced strong, well-recorded, ground shaking, and recent studies have shown an effect on the crustal-scale velocity structure from this earthquake. Nakata and Snieder (2011) report up to ~10% velocity reduction in the upper 100 m from deconvolution of coda of local earthquakes between surface and borehole accelerometers of the KiK-net strong motion network. From this analysis, they infer a reduction in shear strength at depths between the downhole sensor and surface sensor. However, this analysis is limited to regions with colocated surface and borehole stations and only provides information on the depth range between the sensors. This method was later expanded upon by Nakahara (2015) using a similar

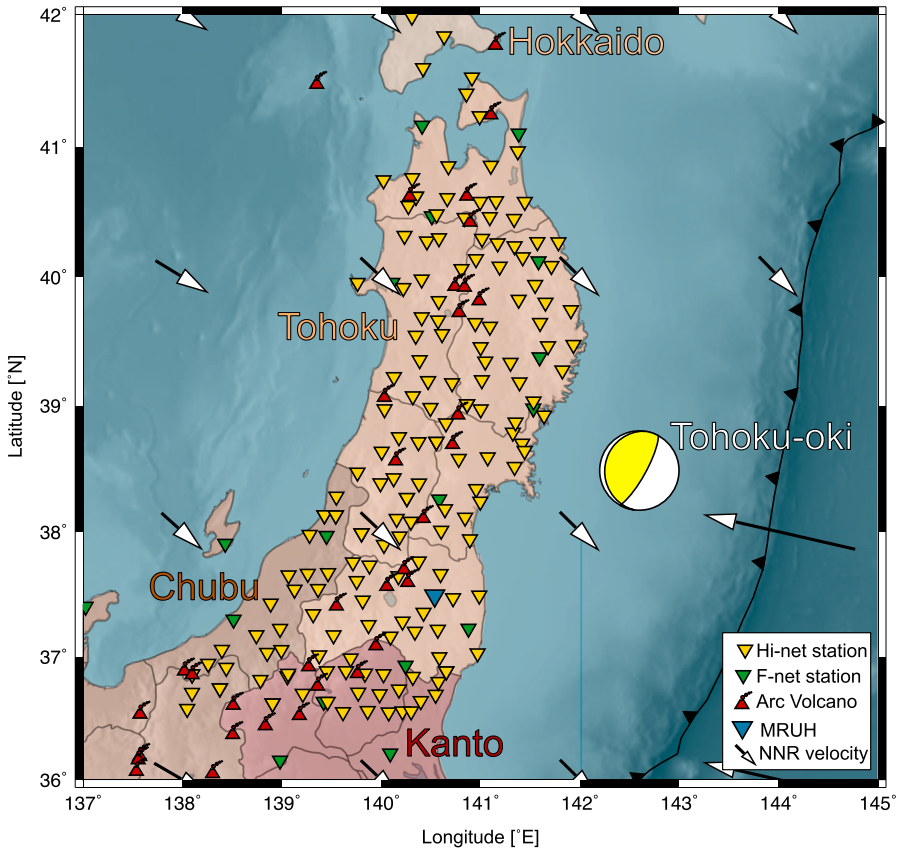

Figure 1. Location of stations used in this study (inverted triangles) and focal mechanism of the Tohoku-oki main shock. Active arc volcanoes are shown as triangles with circles above and arrows show relative plate motion velocity from the No Net Rotation velocity model (DeMets et al., 2010). Regions in Japan (Hokkaido, Tohoku, Kanto, and Chubu) are shown by shaded regions and line segments within those polygons show different Japanese prefectures.

autocorrelation of coda waves from local earthquakes at only surface stations; this analysis returned similarly large delays, on the order of 10–50%.

Green's functions from ambient seismic noise have recently been shown to be stable representations of Earth structure with little variation over time (e.g., Brenguier et al., 2008; Shapiro et al., 2005; Stehly et al., 2006, 2007). This stability has been used to infer reductions in seismic velocity following large earthquakes in Parkfield (Brenguier et al., 2008), Napa Valley (Taira et al., 2015), and northeast Japan (Brenguier et al., 2014; Minato et al., 2012). Minato et al. (2012) found up to ~2% velocity drop in the Kanto region, near the southern end of the Tohoku-oki rupture after the event, from autocorrelations of ambient seismic noise in the 2–5 Hz frequency band. At lower frequencies, 0.1–0.9 Hz, Brenguier et al. (2014) measure up to only ~0.1% shear velocity reduction, but this reduced velocity is observed throughout much of northeast Japan, particularly along the active volcanic arc. This method improves on the deconvolution method because it can be done solely with surface stations, allows measurement between stations, and can resolve variations at different frequency bands with overlapping depth sensitivities.

The above studies provide consistent evidence for a reduction in shear velocity in the crust following the strong shaking of the Tohoku-oki earthquake. These studies also show that the shear velocity returns to its previous values over ~10 days and the velocity reduction is larger with methods which sample shallower depth ranges. These lines of evidence suggest possible mechanisms such as fluid migration (e.g., Brenguier et al., 2014) and reduction in shear strength (e.g., Nakata & Snieder, 2011), possibly due to perturbations of the stress field opening and closing cracks in the continental crust. Here we investigate converted seismic waves isolated by the receiver function method for further evidence of seismic velocity reduction within the continental crust. Receiver functions provide a complementary data set due to their sensitivity

to velocity within the crust and to sharp velocity contrasts with depth. Furthermore, receiver functions can be calculated at various frequency bands to isolate the effects of layers of varying thickness.

2. Methods

2.1. *P* to *S* Receiver Functions

P receiver functions (PRFs) are a common seismological tool used to isolate converted, or scattered, energy beneath a station (e.g., Langston, 1977; Vinnik, 1977). When *P* plane waves are incident upon an almost horizontally layering velocity contrast, a portion of the incident energy is converted into *Sv* wave energy. This converted phase travels to the station at a lag time determined by the depth to the interface (i.e., the distance the converted wave travels) and the V_p/V_s ratio along that raypath. The amplitude of the converted arrival relative to the direct arrival is determined by the impedance contrast at the interface which generated the conversion. Therefore, PRF are sensitive to the seismic velocity structure near a station, but due to their mostly vertical raypaths, they provide complementary sampling to coda interferometry and ambient noise interferometry.

For this analysis, we use the iterative time domain deconvolution method (Ligorria & Ammon, 1999) to deconvolve the vertical component waveform from the radial component, thereby forming the PRF. Additionally, we compute the transverse over vertical receiver function, which has sensitivity to dipping structures and anisotropy. Raw vertical, radial, and transverse components are filtered between 0.02 and 2 Hz before the PRF are computed with a Gaussian filter parameter of 5.0 (time resolution ~0.75 s). This filter has previously been used for resolving features within the crust (e.g., Parker et al., 2015), whereas broader filter parameters (~2.5) are useful for the crust-mantle boundary (e.g., Stanciu et al., 2016) and even broader filters (~0.5–1.0) are best suited for discontinuities within the mantle (e.g., Kawakatsu & Watada, 2007; Porritt & Yoshioka, 2016). This procedure is relatively standard for PRF studies (e.g., Beck & Zandt, 2002; Frassetto et al., 2011; Porritt et al., 2015; Stanciu et al., 2016; Zandt et al., 2003); however, a previous study investigating time-varying structure with PRF chose instead to use a frequency domain damped Wiener deconvolution (Audet, 2010). While differences exist between these two methods, generally, results have been consistent between the different methods. In this case, the iterative method is preferred for its stability with synthetic seismograms.

2.2. Synthetic Seismograms

To test the feasibility of detecting small variations in shear velocity structure with PRF, we compute synthetic receiver functions. Incident *P* plane waves are computed with the raysum code from Frederiksen and Bostock (2000). This method uses a ray theory-based formulation to propagate a Gaussian source function through a stack of layers. The velocity structure of that stack of layers is based on the velocity model used by the Japan Meteorological Agency (JMA) (Figure 2) (Ueno et al., 2002) but converted from a continuous velocity function to a layered model. For all tests, we use a constant horizontal slowness of 0.03 s/km and a source Gaussian function width of 0.75 s. In this section, we address the effects of varying velocity in the upper crustal layers, white noise in the observed data, and contamination by local earthquakes. The effects are quantified by calculation of the two-dimensional anticorrelation (1 − cross correlation) of spectrograms between the reference and test PRF; the spectrograms are limited in time between 0 and 8 s and in frequency between 0.5 and 1 Hz to reduce the effects of signals from the mantle, where we do not expect structural variations on measurable timescales. This frequency band is also chosen because it shows the clearest signal in the analysis by Audet (2010) and captures the earliest time signals in the synthetic reference (Figure 2), and our tests with multiple bands found it to be the least susceptible to noise while still being relatively high frequency.

The effect we are attempting to isolate is a reduction in shear velocity in the crust. Estimates of the velocity reduction vary between as little as 0.01% to as much as 50%. Based on the different methodologies used for these estimates, we expect that the large variations ($>$ ~1%) are primarily limited to the shallow subsurface, but because receiver function sensitivity to shear velocity is highly nonlinear, we test a suite of models with velocity reduction between 0.01% and 10% applied over one to nine layers, each 5 km thick (Figures 3 and S1 in the supporting information). While there is considerable scatter in the results, there is a general pattern of reduced correlation as the velocity reduction is increased and as the number of layers of reduced velocity is

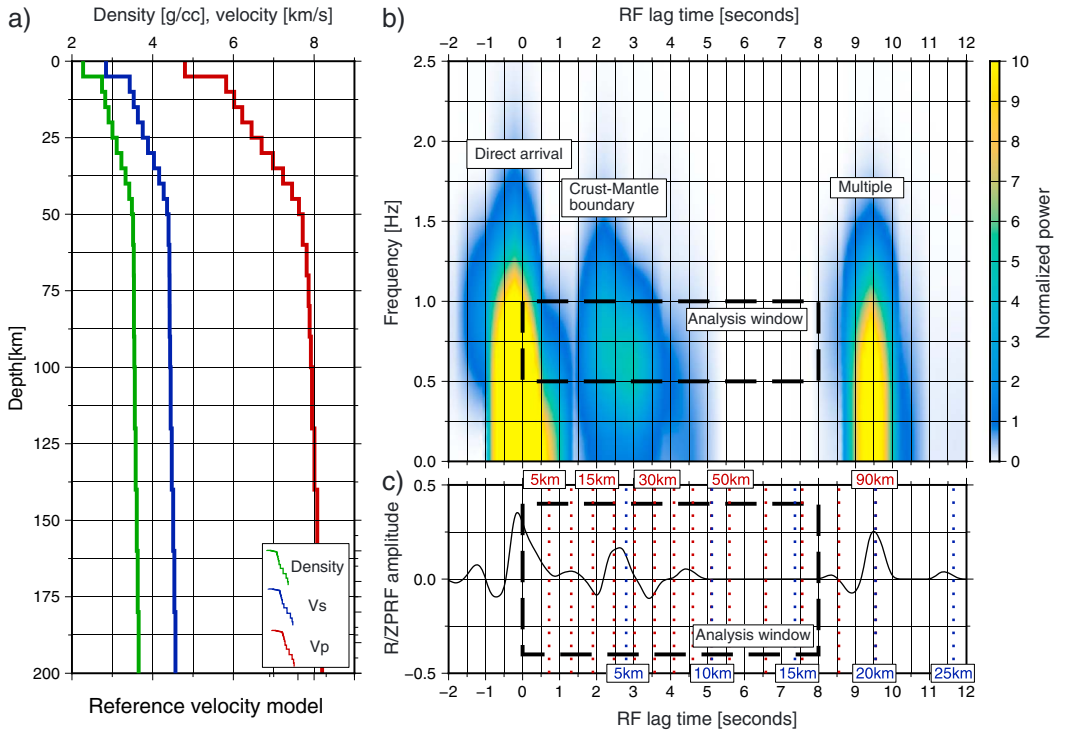

Figure 2. Reference synthetic receiver function. (a) The 1-D velocity model based on the JMA velocity model (Ueno et al., 2002). (b) Spectrogram calculated based on the reference PRF with major conversions labeled. (c) Calculated radial over vertical PRF given a horizontal slowness of 0.03 s/km.

increased (Figure S1). However, there is also a region in this search space where four to nine layers (total depth range of 20–45 km) at 2–6% velocity reduction result in a substantial anticorrelation, on the order of 0.05–0.10.

The effect of random noise is more difficult to constrain, being derived from a stochastic process. We therefore run a set of tests where we add white noise to the reference model seismograms before computing the PRF. The noise is scaled to a maximum of ±1–100% of the peak amplitude and 5,000 realizations are run (Figure S2). For each realization, we calculate the signal-to-noise ratio (SNR). We define the SNR for each waveform as the peak of the envelope from 0 to 3 s relative to the mean of the envelope from −10 to 0 s (where 0 time is the direct *P* arrival). We find in this test that if the peak noise is ~20%, then the expected signal-to-noise ratio (SNR) is ~5 (Figure S2c). Our data set has a mean SNR of ~5, so we rerun this test with a noise range of ±1–20% (Figure 4). These tests show significant scatter, but a clear relation of increased anticorrelation with higher noise levels is observed. This test suggests that the effect of random noise on the anticorrelation is slightly less than the effect of expected structural variations, assuming the data is not dominated by random noise.

The period immediately following the Tohoku-oki earthquake contains significant aftershock activity, and therefore, we expect possible contamination of the PRF by local earthquakes. Visual inspection of the raw waveforms described in section 2.3 below determined that many of the traces analyzed do contain evidence of local earthquakes included in the PRF calculations and here we explore the possible effects of that contamination. To make this test a worst-case scenario, we estimate the local earthquake by starting with the reference model trace, downscaling its amplitude by up to a factor of 10, upscaling its frequency content by reducing the time axis of the added trace, and adding it to the original trace at a variety of relative time offsets (Figures 5 and S3). This test shows that the single biggest effect is the relative amplitude of the local earthquake, but that this effect quickly decays as the amplitude is reduced by half or more. We also observe a substantial effect of the frequency content; as the frequency of the local earthquake increases, the anticorrelation decreases, suggesting that higher-frequency signals have less effect on the PRF. Finally, the relative time delay only has a significant effect if the time delay is relatively short, less than halfway into

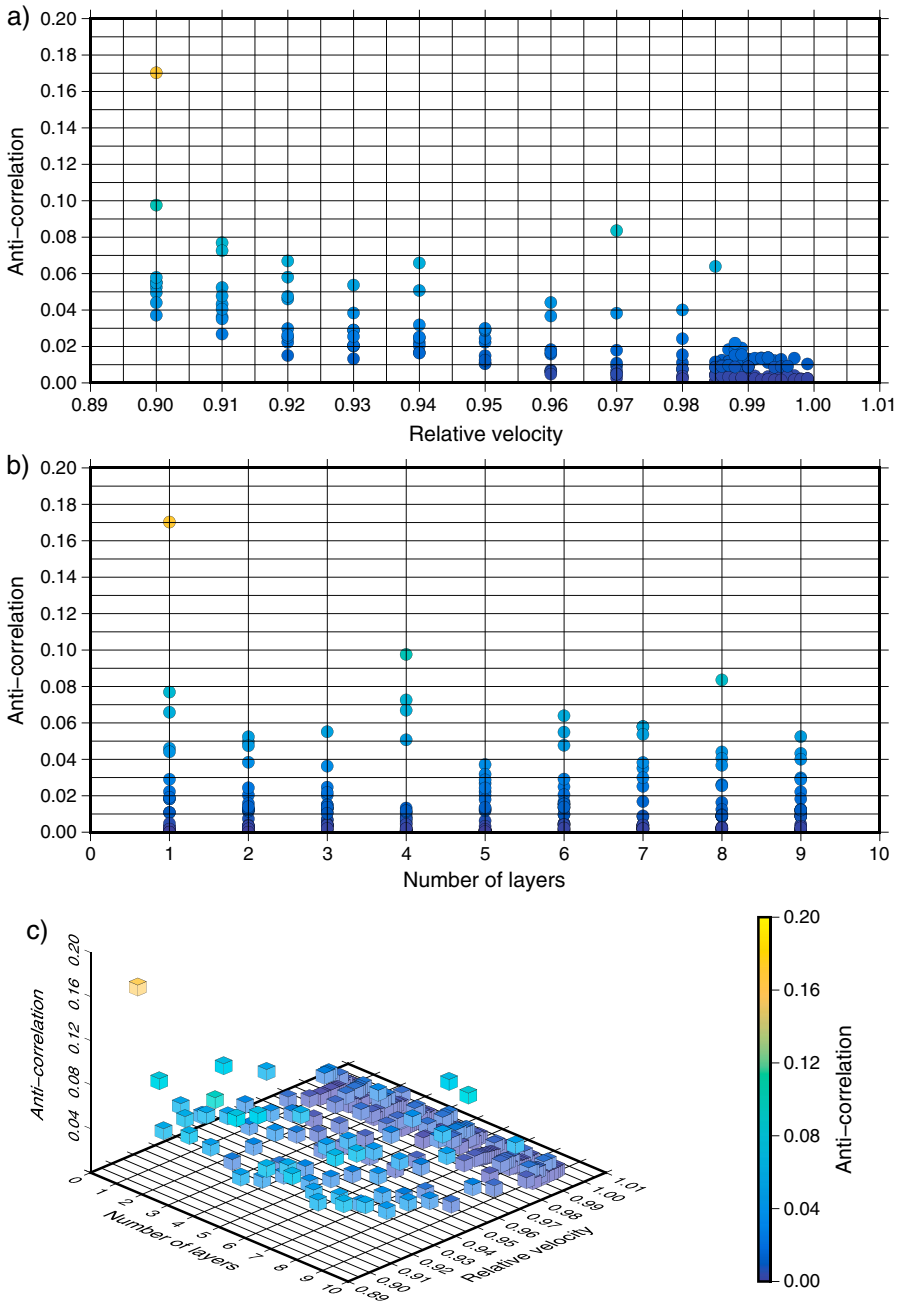

Figure 3. Results of synthetic tests of varied structure. Each panel is a different view of the same 3-D plot. (a) View showing the anticorrelation as a function of the reduction in velocity. (b) View showing the anticorrelation as a function of the number of layers of reduced velocity. (c) View of distribution of anticorrelation versus both velocity reduction and number of layers reduced velocity.

the waveform. This test indicates that later arriving local earthquakes have less of an effect on the final PRF. Overall the effect of local earthquakes in this test can cause an anticorrelation of up to 0.5 in the most extreme case but generally results in anticorrelations of ~0.01–0.06.

2.3. Data

The data for this study comes from the National Research Institute for Earth Science and Disaster Resilience (NIED) of Japan. We use 17 stations of the F-net broadband network and 164 stations of the Hi-net short-period borehole network available in the Tohoku region (Figure 1). We select time windows corresponding

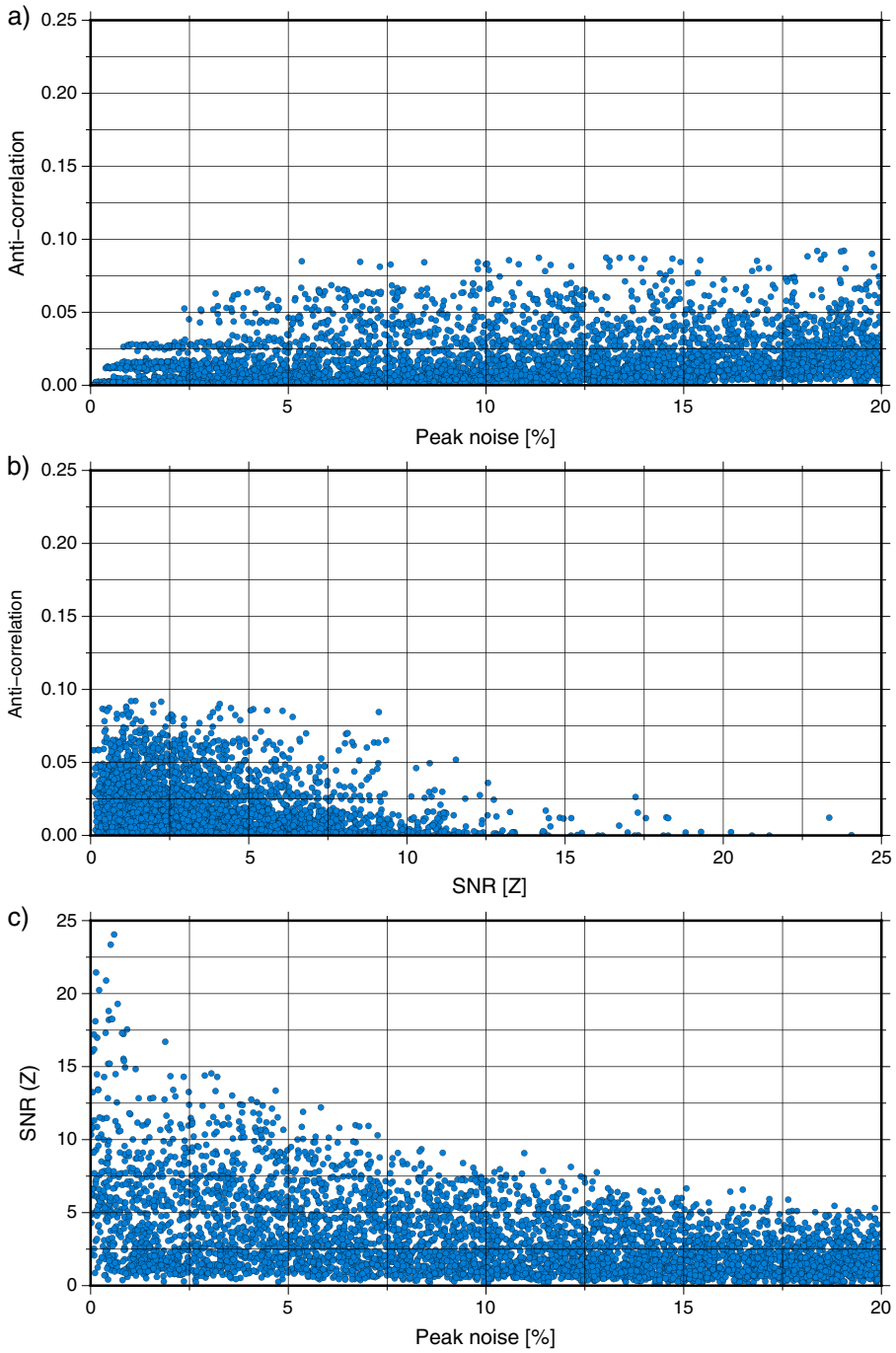

Figure 4. Effect of white noise on the anti-correlation of the PRF. Each blue circle represents one test at a random level of noise. This test has 5,000 realizations of maximum peak-to-peak noise of 20%. (a) Anticorrelation as function of peak noise in test. (b) Anticorrelation as a function of SNR calculated from each realization. (c) SNR as a function of peak noise in the test.

to 10 s before the *P* wave arrival to 100 s after the predicted *P* arrival for 3338 *M*5.5+ earthquakes, with origin times between the years 2004 and 2015, located between 27 and 98° epicentral distance (Figure 6). To avoid noisy seismograms, we focus our analysis on waveforms with minimum SNR of 2 for the vertical component data. From this data set, we compute a reference receiver function at each station as a stack of spectrograms for all PRF recorded during the 12 year period for each of eight overlapping 90° back azimuthal (BAZ) bins. We then estimate the mean and standard deviation of the long-term anticorrelation by sampling 25 (the average

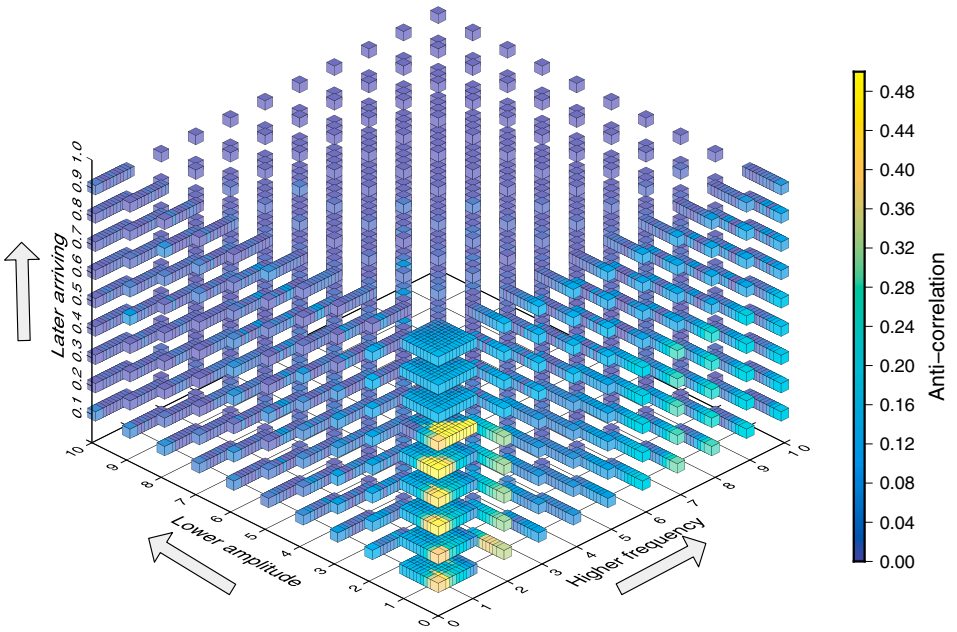

Figure 5. Effect of a synthetic local earthquake on PRF anticorrelation. Anticorrelation is a three-dimensional function of relative amplitude, relative frequency, and where in the waveform the signal is placed. The amplitude axis gives the factor by which the waveform amplitude has been divided. For instance, if the maximum amplitude of the reference trace is 1.0, then at a lower amplitude of 4, the peak amplitude is 0.25. The frequency axis is the factor by which the entire trace is reduced in time before adding to the original trace. For example, if the original trace is 100 s, then at a higher frequency of 4, the added trace has a total time of 25 s but still contains the same pulses as the reference trace. The later arriving axis is when the added trace is added to the reference trace. For a 100 s long reference trace and a 25 s added trace, at an arriving value of 0.1, then the added trace is inserted from 10 s to 35 s.

number of PRF in a 30 day window) random PRF spectrograms, stacking them, and computing the anticorrelation for this sample stack and repeating this test 801 (the number of time windows considered) times (Figure 7, yellow field). We then estimate the anticorrelation as a function of time by jackknife resampling (Tukey, 1958) all PRF in 30 day windows, sliding 5 days at a time, in each of the eight overlapping BAZ bins (Figure 8, orange fields). As with the synthetic analysis, we limit the anticorrelation of spectrograms to 0 to 8 s in time and 0.5 to 1 Hz in frequency. Additionally, we compute the receiver function power for each 90° BAZ, 30 day window, but find no clear trends as described in Audet (2010) and present figures for the receiver function power as a function of time in the supporting information.

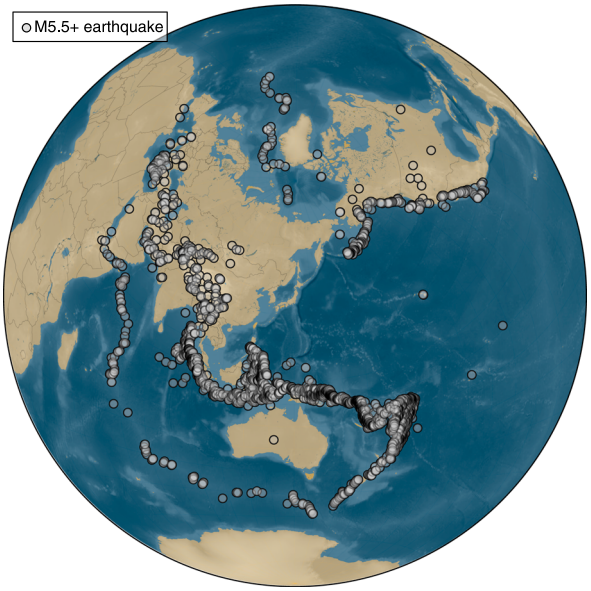

Figure 6. Map of earthquakes used for calculating PRF.

3. Results

Our analysis of synthetic PRF indicate that several factors can nonlinearly interact to create anticorrelations between a reference receiver function and observed receiver functions, and we expect more factors than can be addressed here likely contribute. Nonetheless, there is a nonnegligible effect due to structural variations. Therefore, we assess the variability of the anticorrelation at each station over time using the long-term mean and standard deviation to define periods of statistically significant periods of high or low anticorrelation. High anticorrelation periods may be suspected to be due to temporary velocity changes relative to the long-term structure.

An example of anticorrelation versus time and SNR for Hi-net station MRUH is shown in Figure 7 (see supporting information for a URL to all stations). This station, located in southeastern Tohoku (Figure 1), shows the

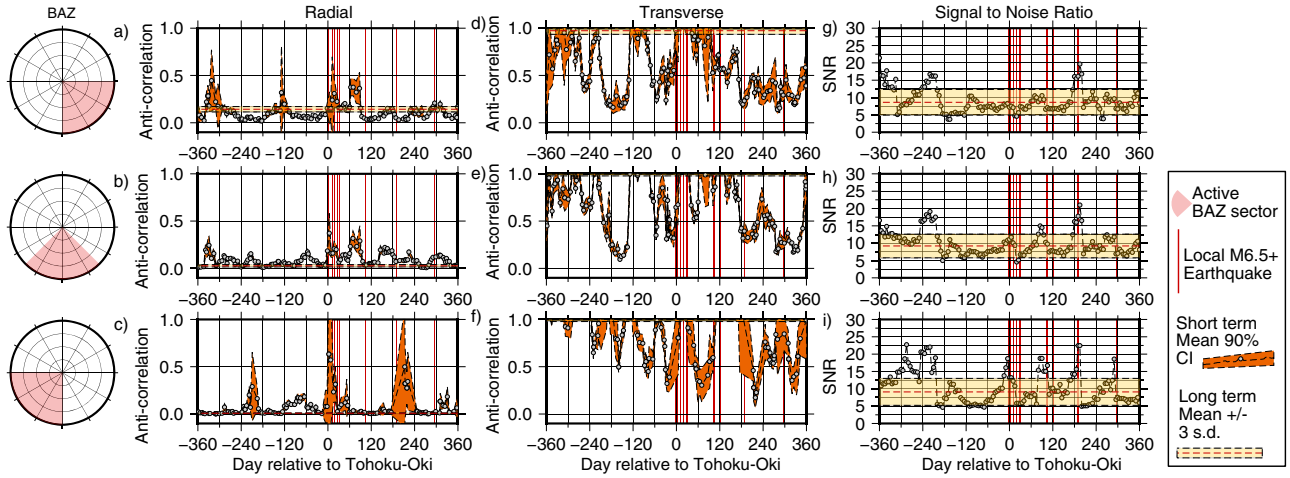

Figure 7. Two years of anticorrelation and SNR versus time at station MRUH. Lines with grey circles on top indicate the measured anticorrelation for each 30 day stack of PRF. Orange field is 90% confidence from jackknife resampling. Red lines indicate local earthquakes with magnitude 6.5 or greater. Tohoku-oki is highlighted as a thickened red line. Yellow fields denote ±3 standard deviations from 15 year bootstrap resampling. (a–c) The radial component anticorrelation at different back azimuthal bins indicated by the red shaded regions within circles. (d–f) The transverse component anticorrelation; (g–i) the corresponding signal-to-noise ratio for the vertical component waveform.

best sampling is from the southeast to southwest (Figure S4), as may also be inferred from the distribution of earthquakes used (Figure 6). Therefore, we can only be confident in the results for these BAZ bins at this station. However, these bins show a statistically significant radial component anticorrelation immediately following the Tohoku-oki earthquake (Figures 7a–7c). We also note a significant anticorrelation ~120 days before Tohoku-oki and ~60 days after for the southeast BAZ bin (Figure 7a) and high anticorrelations ~210 days before and ~225 days after for the southwest BAZ bin (Figure 7c).

As with the synthetic tests, the variability in the anticorrelation can be high and varies for each station. Therefore, when addressing variability across multiple stations, we use the number of standard deviations from the mean at that station as a metric. In Figure 8, we present the mean number of standard deviations averaged over all stations against time for a 2 year time window around Tohoku-oki and the network average SNR. This shows that back azimuths from the southeast, south, and southwest (Figures 8a–8f) have high average anticorrelations, at the 1 standard deviation level, immediately after Tohoku-oki. There are other statistically significant high anticorrelations, such as at ~300 days after Tohoku-oki for back azimuths toward the

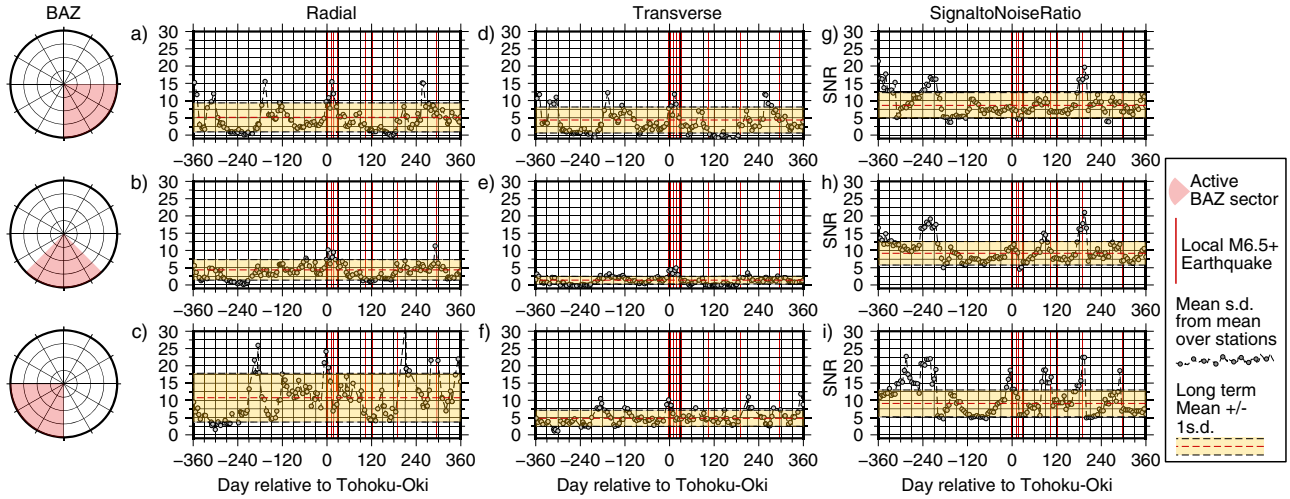

Figure 8. Two years of average number of standard deviations from the (a–c) radial component and (d–f) transverse component mean observed over all stations over time for the three well-sampled back azimuthal bins. Yellow field in the background is the mean ±1 standard deviations over the full 12 year time window. Red vertical lines are *M*6.5+ earthquakes within the region. (g–h) The network average SNR for events with SNR $>$ 2.

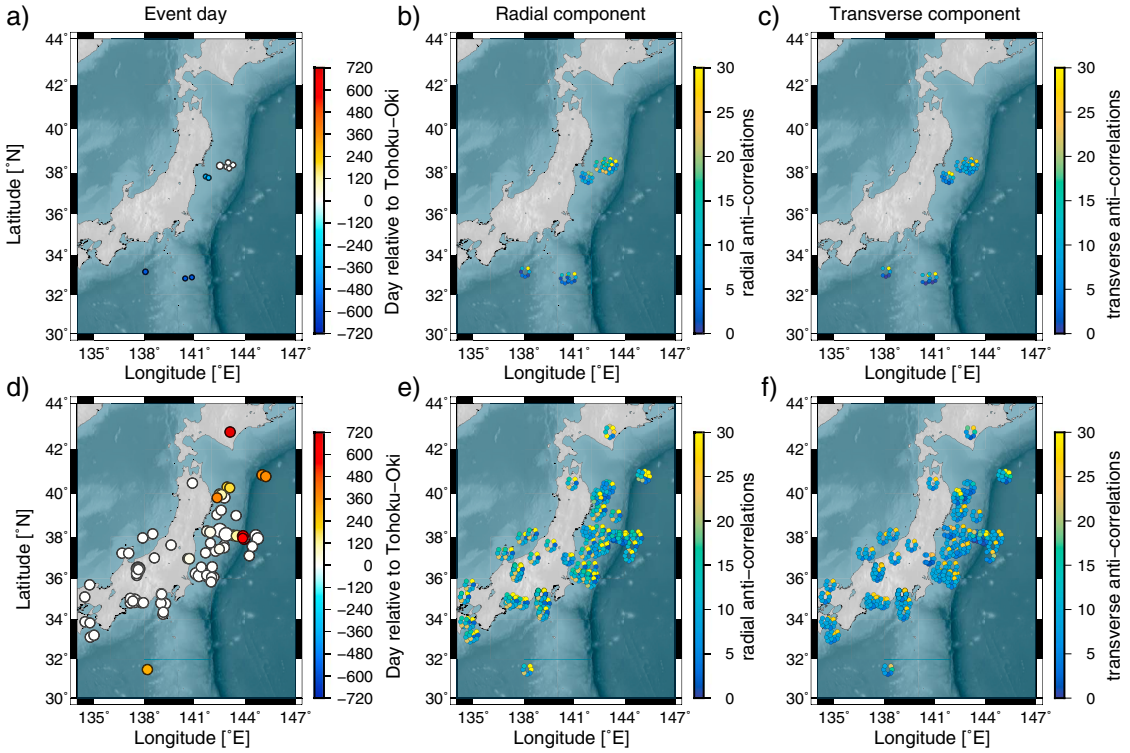

Figure 9. Map views of local earthquakes and radial and transverse anti-correlation standard deviations. Earthquakes have minimum magnitude of 6.5 and depths range from 0 to 360 km. (a) Origin time relative to Tohoku-oki for earthquakes up to 720 days before Tohoku-oki. (b) Average number of radial component standard deviations from the mean for each BAZ bin plotted at 0.2° from the earthquake origin for events prior to Tohoku-oki. (c) Average number of transverse component standard deviations from the mean for each BAZ bin plotted at 0.2° from the earthquake origin for events prior to Tohoku-oki. (d) Origin time relative to Tohoku-oki for earthquakes up to 720 days after Tohoku-oki. (e) Average number of radial component standard deviations from the mean for each BAZ bin plotted at 0.2° from the earthquake origin for events after Tohoku-oki. (f) Average number of transverse component standard deviations from the mean for each BAZ bin plotted at 0.2° from the earthquake origin for events after Tohoku-oki.

south (Figure 8b). We further note that as with Figure 7, there is an apparent drop in SNR, but it is still within 1 standard deviation.

In addition to analyzing the PRF anticorrelation in time, we can also address the information in the spatial domain. Figure 9 shows the spatial distribution of large local earthquakes colored by day relative to Tohoku-oki and the same metric presented in Figure 8. The 2 years before Tohoku-Oki (Figures 9a–9c) shows relatively low anticorrelations for earthquakes that occurred 120 days or longer before Tohoku-oki, particularly with the southern BAZ bins. However, earthquakes which occurred after Tohoku-oki's origin time show relatively high anticorrelations (Figures 9d–9f) if they occurred within ~120 days of Tohoku-oki; later earthquakes show generally lower mean anticorrelations. Many of these estimates come from the same set of receiver functions, so they may be indicating a signal limited to a relatively short time window around Tohoku-oki, which happens to correspond to increased seismicity from aftershock activity.

4. Discussion

Our results are consistent with previous studies which show that the crust is susceptible to temporal changes in seismic velocity due to strong ground shaking. These changes last for time periods on the order of a week to 3 months (e.g., Minato et al., 2012) before the seismic velocity returns to near its previous value. This requires a mechanism which could produce a decline in the seismic velocity within the crust within this timescale. Possible mechanisms that have been proposed include volcanic fluid migration (Brenguier et al., 2014) and reduction in shear strength (e.g., Nakata & Snieder, 2011).

Receiver functions can vary significantly based on their raypath through the crust. Therefore, we have so far considered variation with back azimuth to provide information about different swaths of the crust (e.g.,

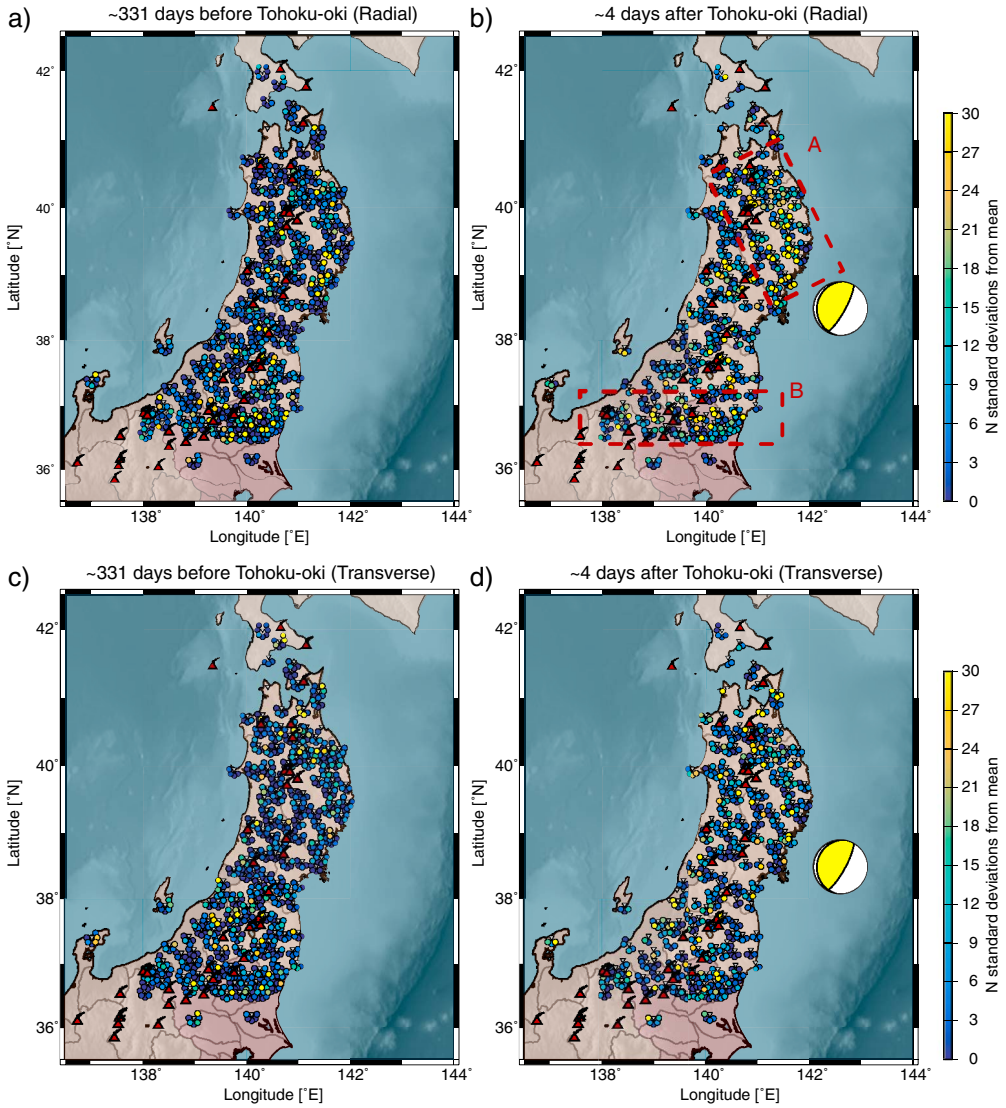

Figure 10. Average number of standard deviations from the mean anticorrelation (a, c) before and (b, d) after Tohoku-oki. Boxes A and B indicate regions of high anticorrelation. Figures 10a and 10b are for the radial component, and Figures 10c and 10d are the transverse component.

Agostinetti & Chiarabba, 2008). Furthermore, because transverse component receiver functions can indicate dipping structures or anisotropy, they provide valuable structural information. However, the transverse component receiver functions can have a high mean and standard deviation in the anticorrelations (Figures 7d–7f). Therefore, we cannot have high confidence in transverse component results.

Figure 10 shows map views of radial and transverse component anticorrelation for a 30 day time window immediately following Tohoku-oki and an earlier time window without a large earthquake preceding it. In this case, each BAZ bin is plotted with a slight moveout from the recording station to indicate the approximate spatial location where these signals are being generated. The pattern of high anticorrelation (greater than ~3–4 standard deviations above the station mean) appears to follow along the arc, consistent with the ambient noise based evidence of Brenguier et al. (2014), and we can therefore infer some of this signal is the result of fluid migration throughout the crust. Based on our synthetic tests showing a peak in the anticorrelation when the top four layers have reduced velocity and the relatively narrow Gaussian width used here, we infer that this signal occurs mostly within the upper 20 km. This depth range is consistent with prior expectations for magmatic plumbing systems (e.g., Karlstrom et al., 2009; Porritt et al., 2011) and includes not

only the main magma chamber itself but also the pressure zone over which magma chambers are able to capture nearby dikes (Karlstrom et al., 2009). From this line of reasoning, we infer that the velocity change may not just be direct fluid migration but may also have a dynamic stress component through pressure changes.

In addition to the arc, we identify two regions of high anticorrelation (boxes A and B). Regions A and B are at the start and end of the rupture plane, respectively. This suggests there is significant induced stress in these regions. The southwest edge of box A corresponds to the Oga-Ojika Tectonic Line (OOTL) (Hashimoto & Jackson, 1993; Mogi, 1985). This feature was identified due to an alignment of earthquake epicenters between the Oga Peninsula and the Ojika Peninsula (Mogi, 1985) and has been used as a block boundary for geodetic modeling (e.g., Hashimoto & Jackson, 1993; Loveless & Meade, 2010). While the high anticorrelation in this region may reflect crustal fluid migration, we consider it possible that this also reflects a reduction in shear strength (e.g., Nakata & Snieder, 2011) and/or a reorganization of stress in the region. This interpretation is supported by an increase in crustal seismicity along the OOTL in the JMA earthquake catalog. Furthermore, the observation of mostly strike-slip seismicity along the OOTL following the main shock (e.g., Yoshida et al., 2012) suggests that reduction in normal stress due to increased pore pressure may not be responsible; rather, a reduction in shear strength holding the fault locked or an increase in stress may account for the increased seismicity.

The argument for fluid migration proposed by Brenguier et al. (2014) depends on a qualitative correlation between velocity drop and locations of arc volcanoes. This argument is further supported by evidence presented in Okada et al. (2015) showing migrations of seismicity within swarms, which could be fit by a diffusion relation with a permeability of $\sim 10^{-15}$ m^2. However, these two studies differ on the spatial extent of fluid migration within the crust. The swarm seismicity is localized to nine locations, whereas the velocity drop is a continuous function along the arc; the anticorrelation maps in Figure 10 show a localized view of velocity change, consistent with the swarm seismicity. We therefore infer that fluid migration occurred primarily within highly susceptible regions, such as fault systems or volcanic plumbing systems.

While the above suggests there may be Earth system processes responsible for observations of high anticorrelation, we note that our synthetic tests reveal several factors can contribute. The most notable effects we expect are random noise and local earthquakes, both of which are clearly present in our data immediately following Tohoku-oki and throughout the 12 year time window of analysis. However, we have also identified several other time periods of potential velocity change by sampling relatively short time windows (110 s per sample PRF) over a time span of 12 years. This result suggests that other analyses, such as ambient noise, if run over longer time periods, may also recover measurable velocity changes through time. Additionally, future analyses may be able to include receiver function data in structural inversions to address temporal variations in fully three-dimensional velocity models.

5. Conclusions

Here we have shown evidence for variability in measured PRF signals following the strong ground shaking of Tohoku-oki, other large earthquakes, and during the interseismic period. Synthetic tests indicate that a drop in crustal seismic velocity is likely to be the largest contributing factor, but other factors can also be significant. Observations of anticorrelations show high variability over time and between stations suggesting an influence of spatial seismic susceptibility and time-dependent processes. However, there does appear to be wide-spread high anticorrelations immediately following Tohoku-oki. Many of the stations with high anticorrelation are near active arc volcanoes suggesting the role of magmatic processes and the regions of high anticorrelation near the start and end of the rupture plane suggests a temporary drop in shear strength or an increase in shear stress.

Acknowledgments

We thank Meghan S. Miller for informal comments on this manuscript and two formal anonymous reviewers for improving this manuscript. Funding for this project was provided by the Research Center for Urban Safety and Security of Kobe University which supported R. W. Porritt during a visit to Kobe University. This work was also partially supported by JSPS KAKENHI grant 15H01140. Waveform data were provided by the Japan National Research Institute for Earth Science and Disaster Resilience, and we thank Makoto Matsubara for help with acquiring the data. Additional analysis figures available for all stations at RWP's website: https://robporritt.wordpress.com/tohoku_oki_and_time_varying_prf/. Earthquake epicenters and the reference velocity model provided by the Japan Meteorological Agency. Figures made with Generic Mapping Tools (GMT) (Wessel & Smith, 1998).

References

Agostinetti, N. P., & Chiarabba, C. (2008). Seismic structure beneath Mt. Vesuvius from receiver function analysis and local earthquakes tomography: Evidences for location and geometry of the magma chamber. *Geophysical Journal International*, *175*(3), 1298–1308. https://doi.org/10.1111/j.1365-246X.2008.03868.x

Audet, P. (2010). Temporal variations in crustal scattering structure near Parkfield, California, using receiver functions. *Bulletin of the Seismological Society of America*, *100*(3), 1356–1362. https://doi.org/10.1785/0120090299

Beck, S., & Zandt, G. (2002). The nature of orogenic crust in the central Andes. *Journal of Geophysical Research: Solid Earth*, *107*(B10), 2230. https://doi.org/10.1029/2000JB000124

Brenguier, F., Campillo, M., Hadziioannou, C., Shapiro, N. M., Nadeau, R. M., & Larose, E. (2008). Postseismic relaxation along the San Andreas Fault at Parkfield from continuous seismological observations. *Science*, *321*(5895), 1478–1481. https://doi.org/10.1126/science.1160943

Brenguier, F., Campillo, M., Takeda, T., Aoki, Y., Shapiro, N. M., Briand, X., … Miyake, H. (2014). Mapping pressurized volcanic fluids from induced crustal seismic velocity drops. *Science*, *345*(6192), 80–82. https://doi.org/10.1126/science.1254073

DeMets, C., Gordon, R. G., & Argus, D. F. (2010). Geologically current plate motions. *Geophysical Journal International*, *181*(1), 1–80. https://doi.org/10.1111/j.1365-246X.2009.04491.x

Frassetto, A. M., Zandt, G., Gilbert, H., Owens, T. J., & Jones, C. H. (2011). Structure of the Sierra Nevada from receiver functions and implications for lithospheric foundering. *Geosphere*, *7*(4), 898–921. https://doi.org/10.1130/GES00570.1

Frederiksen, A. W., & Bostock, M. G. (2000). Modelling teleseismic waves in dipping anisotropic structures. *Geophysical Journal International*, *141*(2), 401–412. https://doi.org/10.1046/j.1365246x.2000.00090.x

Hashimoto, M., & Jackson, D. D. (1993). Plate tectonics and crustal deformation around the Japanese Islands. *Journal of Geophysical Research: Solid Earth*, *98*(B9), 16,149–16,166. https://doi.org/10.1029/93JB00444

Hayes, G. P. (2011). Rapid source characterization of the 2011 M_w 9.0 off the Pacific coast of Tohoku Earthquake. *Earth, Planet and Space*, *63*(4). https://doi.org/10.5047/eps.2011.05.012

Karlstrom, L., Dufek, J., & Manga, M. (2009). Organization of volcanic plumbing through magmatic lensing by magma chambers and volcanic loads. *Journal of Geophysical Research: Solid Earth*, *114*, B10204. https://doi.org/10.1029/2009JB006339

Kawakatsu, H., & Watada, S. (2007). Seismic evidence for deep-water transportation in the mantle. *Science*, *316*(5830), 1468–1471. https://doi.org/10.1126/science.1140855

Kiser, E., & Ishii, M. (2012). The March 11, 2011 Tohoku-oki earthquake and cascading failure of the plate interface. *Geophysical Research Letters*, *39*, L00G25. https://doi.org/10.1029/2012GL051170

Koper, K. D., Hutko, A. R., Lay, T., Ammon, C. J., & Kanamori, H. (2011). Frequency-dependent rupture process of the 2011 M_w 9.0 Tohoku Earthquake: Comparison of short-period *P* wave backprojection images and broadband seismic rupture models. *Earth, Planet and Space*, *63*(16). https://doi.org/10.5047/eps.2011.05.026

Langston, C. A. (1977). Corvallis, Oregon, crustal and upper mantle receiver structure from teleseismic *P* and *S* waves. *Bulletin of the Seismological Society of America*, *67*(3), 713–724.

Lay, T., Ammon, C. J., Kanamori, H., Xue, L., & Kim, M. J. (2011). Possible large near-trench slip during the 2011 M_w 9.0 off the Pacific coast of Tohoku Earthquake. *Earth, Planets and Space*, *63*(32). https://doi.org/10.5047/eps.2011.05.033

Ligorria, J. P., & Ammon, C. J. (1999). Iterative deconvolution and receiver-function estimation. *Bulletin of the Seismological Society of America*, *89*(5), 1395–1400.

Loveless, J. P., & Meade, B. J. (2010). Geodetic imaging of plate motions, slip rates, and partitioning of deformation in Japan. *Journal of Geophysical Research*, *115*, B02410. https://doi.org/10.1029/2008JB006248

Meng, L., Inbal, A., & Ampuero, J.-P. (2011). A window into the complexity of the dynamic rupture of the 2011 M_w 9 Tohoku-oki earthquake. *Geophysical Research Letters*, *38*, L00G07. https://doi.org/10.1029/2011GL048118

Minato, S., Tsuji, T., Ohmi, S., & Matsuoka, T. (2012). Monitoring seismic velocity change caused by the 2011 Tohoku-oki earthquake using ambient noise records. *Geophysical Research Letters*, *39*, L09309. https://doi.org/10.1029/2012GL051405

Mogi, K. (1985). *Earthquake prediction* (pp. 355). San Diego, CA: Academic.

Nakahara, H. (2015). Auto correlation analysis of coda waves from local earthquakes for detecting temporal changes in shallow subsurface structures: The 2011 Tohoku-oki, Japan earthquake. *Pure and Applied Geophysics*, *172*(213). https://doi.org/10.1007/s00024-014-0849-0

Nakata, N., & Snieder, R. (2011). Near-surface weakening in Japan after the 2011 Tohoku-oki earthquake. *Geophysical Research Letters*, *38*, L17302. https://doi.org/10.1029/2011GL048800

Okada, T., Matsuzawa, T., Umino, N., Yoshida, K., Hasegawa, A., Takahashi, H., … Miyamachi, H. (2015). Hypocenter migration and crustal seismic velocity distribution observed for the inland earthquake swarms induced by the 2011 Tohoku-Oki earthquake in NE Japan: Implications for crustal fluid distribution and crustal permeability. *Geofluids*, *15*(1–2), 293–309. https://doi.org/10.1111/gfl.12112

Parker, E. H., Hawman, R. B., Fischer, K. M., & Wagner, L. S. (2015). Constraining lithologic variability along the Alleghanian detachment in the southern Appalachians using passive-source seismology. *Geology*, *43*(5), 431–434. https://doi.org/10.1130/G36517.1

Pollitz, F. F., Bürgmann, R., & Banerjee, P. (2011). Geodetic slip model of the 2011 *M*9.0 Tohoku earthquake. *Geophysical Research Letters*, *38*, L00G08. https://doi.org/10.1029/2011GL048632

Porritt, R. W., Allen, R. M., Boyarko, D. C., & Brudzinski, M. R. (2011). Investigation of Cascadia segmentation with ambient noise tomography. *Earth and Planetary Science Letters*, *309*(1–2), 67–76. https://doi.org/10.1016/j.epsl.2011.06.026

Porritt, R. W., Miller, M. S., & Darbyshire, F. A. (2015). Lithospheric architecture beneath Hudson Bay. *Geochemistry, Geophysics, Geosystems*, *16*, 2262–2275. https://doi.org/10.1002/2015GC005845

Porritt, R. W., & Yoshioka, S. (2016). Slab pileup in the mantle transition zone and the 30 May 2015 Chichi-jima earthquake. *Geophysical Research Letters*, *43*, 4905–4912. https://doi.org/10.1002/2016GL068168

Shapiro, N. M., Campillo, M., Stehly, L., & Ritzwoller, M. H. (2005). High-resolution surface-wave tomography from ambient seismic noise. *Science*, *307*(5715), 1615–1618. https://doi.org/10.1126/science.1108339

Simons, M., Minson, S. E., Sladen, A., Ortega, F., Jiang, J., Owen, S. E., … Webb, F. H. (2011). The 2011 magnitude 9.0 Tohoku-oki earthquake: Mosaicking the megathrust from seconds to centuries. *Science*, *332*(6036), 1421–1425. https://doi.org/10.1126/science.1206731

Stanciu, A. C., Russo, R. M., Mocanu, V. I., Bremner, P. M., Hongsresawat, S., Torpey, M. E., … Hole, J. A. (2016). Crustal structure beneath the Blue Mountains terranes and cratonic North America, eastern Oregon, and Idaho, from teleseismic receiver functions. *Journal of Geophysical Research: Solid Earth*, *121*, 5049–5067. https://doi.org/10.1002/2016JB012989

Stehly, L., Campillo, M., & Shapiro, N. M. (2006). A study of the seismic noise from its long-range correlation properties. *Journal of Geophysical Research: Solid Earth*, *111*, B10306. https://doi.org/10.1029/2005JB004237

Stehly, L., Campillo, M., & Shapiro, N. M. (2007). Traveltime measurements from noise correlation: Stability and detection of instrumental time-shifts. *Geophysical Journal International*, *171*(1), 223–230. https://doi.org/10.1111/j.1365246X.2007.03492.x

Taira, T., Brenguier, F., & Kong, Q. (2015). Ambient noise-based monitoring of seismic velocity changes associated with the 2014 M_w 6.0 South Napa earthquake. *Geophysical Research Letters*, *42*, 6997–7004. https://doi.org/10.1002/2015GL065308

Tukey, J. W. (1958). Bias and confidence in not quite large samples. *The Annals of Mathematical Statistics*, *29*, 614–623. https://doi.org/10.1214/aoms/1177706647

Ueno, H., Hatakeyama, S., Aketagawa, T., Funasaki, J., & Hamada, N. (2002). Improvement of hypocenter determination procedures in the Japan Meteorological Agency. *Quarterly Journal of Seismology*, *65*, 123–134.

Wessel, P., & Smith, W. H. F. (1998). New, improved version of the generic mapping tools released. *EOS, Transactions American Geophysical Union*, *79*, 579.

Vinnik, L. P. (1977). Detection of waves converted from *P* to *SV* in the mantle. *Physics of the Earth and Planetary Interiors*, *15*(1), 39–45. https://doi.org/10.1016/0031-9201(77)90008-5

Yoshida, K., Hasegawa, A., Okada, T., Iinuma, T., Ito, Y., & Asano, Y. (2012). Stress before and after the 2011 great Tohoku-oki earthquake and induced earthquakes in inland areas of eastern Japan. *Geophysical Research Letters*, *39*, L03302. https://doi.org/10.1029/2011GL049729

Zandt, G., Leidig, M., Chmielowski, J., Baumont, D., & Yuan, X. (2003). Seismic detection and characterization of the Altiplano-Puna Magma Body, Central Andes. *Pure and Applied Geophysics*, *160*(3), 789–807. https://doi.org/10.1007/PL00012557